# Optical potentials for nuclear level structures and nucleon interactions data of tin isotopes based on the soft-rotator model

Jeong-Yeon Lee,[1,*] Insik Hahn,[2] Yeongduk Kim,[3] Seung-Woo Hong,[1,4] Satoshi Chiba,[5,6] and Efrem Sh. Soukhovitskii[7]

[1]*Department of Physics, Sungkyunkwan University, Suwon 440-746, Korea*

[2]*Department of Science Education, Ewha Womans University, Seoul 120-750, Korea*

[3]*Department of Physics, Sejong University, Seoul 140-747, Korea*

[4]*Department of Energy Science, Sungkyunkwan University, Suwon 440-746, Korea*

[5]*Japan Atomic Energy Agency, Tokai-mura, Ibaraki-ken 319-1195, Japan*

[6]*National Astronomical Observatory of Japan, Mitaka, Tokyo 181-8588, Japan*

[7]*Joint Institute for Energy and Nuclear Research-Sosny, Minsk-Sosny 220109, Belarus*

(Received 23 February 2009; published 23 June 2009)

The soft-rotator model is applied to self-consistent analyses of the nuclear level structures and the nucleon interaction data of the even-even Sn isotopes, $^{116}$Sn, $^{118}$Sn, $^{120}$Sn, and $^{122}$Sn. The model successfully describes low-lying collective levels of these isotopes, which exhibit neither typical rotational nor harmonic vibrational structures. The experimental nucleon interaction data—total neutron cross sections, proton reaction cross sections, and nucleon elastic and inelastic scattering data—are well described up to 200 MeV in a coupled-channels optical model approach. For the calculations, nuclear wave functions for the Sn isotopes are taken from the nonaxial soft-rotator model with the model parameters adjusted to fit the measured low-lying collective level structures. We find that the $\beta_2$ and $\beta_3$ deformations for incident protons are larger than those for incident neutrons by ∼15%, which is clear evidence of the deviation from the pure collective model for these isotopes.

DOI: 10.1103/PhysRevC.79.064612 PACS number(s): 25.40.−h, 21.60.Ev, 24.10.Ht, 27.60.+j

## I. INTRODUCTION

Analyses and understanding of nuclear level structures and nucleon interaction data for Sn isotopes are not only interesting but also useful, because Sn is a component of nuclear reactor materials and a candidate material for superconducting magnets in fusion reactors. From the theoretical perspective, the Sn isotopes have usually been considered as vibrational nuclei; therefore, most calculations of nucleon interaction cross sections for these nuclei using coupled-channels or distorted-wave Born approximation (DWBA) formalism have usually been performed using the harmonic vibrational model. However, the energy splittings of the yrast $0^+$, $2^+$, $4^+$, and $6^+$ levels for these nuclei are too irregular to be considered as harmonic vibrational states. Sn isotopes are single-closed-shell nuclei of $Z = 50$ with many interesting features. Therefore, it is interesting to see whether the calculations using a self-consistent coupled-channels (CC) optical model [1] may produce different nuclear deformations for different external probes (protons or neutrons) for Sn isotopes, as predicted in Ref. [2].

In the present work, we employ the soft-rotator model [3,4] to describe the collective level structures of the even-even $^{116-122}$Sn isotopes. The present soft-rotator model includes the nonaxial quadrupole, octupole, and hexadecapole deformations, and the $\beta_2$, $\beta_3$, and $\gamma$ vibrations [3,4]. The model allows us to identify not only collective levels of positive parity bands but also those of negative parity bands, which are associated with octupole surface vibrations. The essential difference between the present optical model coupled-channels approach and the ones that conventionally use rotational or vibrational models [1] is that we consider, simultaneously, rotations and quadrupole and octupole vibrations of nonaxial nuclei. Therefore, our expressions for the coupling matrix elements involve the corresponding overlap integrals of the wave functions over the appropriate deformation, which describes vibrational motions. This enhances the coupling of channels in comparison with the results predicted by rotational model cases [1]. Conventional CC models need to keep different deformations for different pairs of levels to describe experimental cross sections for excited levels, while in our model such difference appears naturally through "effective" deformations. Therefore, the softness of a nucleus leads to redistribution of the flux of scattered particles among the channels. Furthermore, the present soft-rotator model is self-consistent in that the parameters of the nuclear Hamiltonian are determined by fitting the calculated energies of collective levels to the evaluated nuclear structure data and that the wave functions from such a nuclear Hamiltonian with parameters describing low-lying collective levels are used to build coupling in the coupled-channels optical model calculations. This model has been quite successful in describing the low-lying collective excitations, nucleon interaction data, and electromagnetic transitions for a heavy rotational nucleus of $^{238}$U [5], a light nucleus $^{12}$C [6,7], and the vibrational nuclei $^{58}$Ni [8], $^{56}$Fe [9], and $^{52}$Cr [10]. Since the coupling strength involved in such CC optical model calculations already takes into account nuclear level structure effects, the optical model parameters are expected to be free from such effects, and thus this model is suitable for the systematic determination of optical model parameters when coupled-channel effects are significant.

It is our aim to consistently describe the collective nuclear structures and nucleon scattering properties of the $^{116-122}$Sn even-even isotopes in the framework of the self-consistent

*yeonis@skku.edu

 

soft-rotator model. Section II sketches the soft-rotator model applied to the analysis of the collective level structures of the $^{116-122}$Sn even-even isotopes. In Sec. III, CC optical model calculations based on wave functions from the soft-rotator nuclear model are applied to analyze all nucleon interaction data available for the Sn even-even isotopes. Section IV shows the dependence of Sn isotopes deformations on the incident probe. Conclusions follow in Sec. V.

## II. DESCRIPTIONS OF LOW-LYING COLLECTIVE LEVEL STRUCTURES FOR Sn EVEN-EVEN ISOTOPES

The observed low-lying collective levels of even-even Sn isotopes with $A = 116$, 118, 120, and 122 are described by adjusting the Hamiltonian parameters in the soft-rotator nuclear model. The assignment of the soft-rotator model quantum numbers to the experimental low-lying collective Sn levels is done by following Ref. [11]. We take the first levels with spins and parities $J^\pi = 0_1^+, 2_1^+, 4_1^+$ as the members of the ground state (g.s.) rotational band with $K \simeq 0, n_\beta = n_\gamma = 0$. The first $J^\pi = 3_1^+$ levels are assigned as members of the $K \simeq 2, n_\beta = n_\gamma = 0$ band. The second $J^\pi = 0_2^+$ levels are taken as the heads of the $K \simeq 0, n_\beta = 1, n_\gamma = 0$ band. The third $J^\pi = 0_3^+$ and $J^\pi = 2_3^+$ levels are considered as levels of the $K \simeq 0, n_\beta = 0, n_\gamma = 1$ positive parity rotational band, and the first $3_1^-$ levels as collective levels of $K \simeq 0$ negative parity band associated with octupole surface vibrations. Such assignments allow us to find soft-rotator Hamiltonian parameters. The nuclear Hamiltonian parameters for $^{116,118,120,122}$Sn are given in Table I. (The detailed definition of these parameters can be found in Refs. [4,6].) One can see that Sn isotopes are very soft to $\beta_2$ and $\gamma$ deformations. The softness $\mu_{\beta_{20}}$ is found to be 3.306 for $^{116}$Sn and is smoothly decreasing to 2.324 for $^{122}$Sn, thus implying that Sn isotopes are very soft but become relatively more rigid as mass number increases.

Figure 1 compares the theoretically predicted nuclear energy levels with the experimental ones for the isotopes $^{116}$Sn, $^{118}$Sn ,$^{120}$Sn, and $^{122}$Sn. For each Sn isotope, we can produce nine levels out of approximately 10–12 levels observed up to 2.4 MeV in excitation energy. In all these isotopes, we are unable to produce the energy sequence of $5_1^-$ levels, which are observed experimentally at energies lower than $3_1^-$ ones. Theoretically predicted energies of Sn levels other than $5_1^-$ are in good agreement with the experimental ones. Rotational structures are not very prominent in Sn isotopes; nevertheless, for each isotope we can describe at least five first low-lying collective levels, with average energy prediction accuracy better than 5%, and some other levels lying above, necessary for creating the coupling scheme of coupled-channel calculations.

TABLE I. Nuclear Hamiltonian parameters adjusted to reproduce the experimental nuclear energy levels for the four even-even Sn isotopes. $\hbar\omega_0$ is in MeV; other quantities have no dimension.

| | $^{116}$Sn | $^{118}$Sn | $^{120}$Sn | $^{122}$Sn |
|---|---|---|---|---|
| $\hbar\omega_0$ | 1.0005 | 1.0228 | 1.0610 | 1.0996 |
| $\mu_{\beta_{20}}$ | 3.3060 | 3.0160 | 2.5955 | 2.3241 |
| $\mu_{\gamma_0}$ | 4.7600 | 4.7600 | 4.7600 | 4.7600 |
| $\gamma_0$ | 0.5632 | 0.4310 | 0.4120 | 0.4011 |
| $a_{32}$ | 0.0049 | 0.0049 | 0.0049 | 0.0049 |
| $\gamma_4$ | 0.0939 | 0.0939 | 0.0939 | 0.0939 |
| $\delta_4$ | 0.6972 | 0.6972 | 0.6972 | 0.6972 |
| $a_{42}$ | 0.3500 | 0.3500 | 0.3500 | 0.3500 |
| $\mu_\epsilon$ | 1.9310 | 1.4554 | 1.1829 | 1.0665 |
| $\eta$ | 0.0422 | 0.0276 | 0.0802 | 0.0473 |
| $\delta_n$ | 1.4016 | 1.7318 | 2.0042 | 2.1818 |

## III. OPTICAL MODEL CALCULATION FOR NUCLEON INTERACTION DATA

### A. Nuclear shapes and nuclear optical potential

We assume that the excited states observed in even-even nonspherical nuclei can be described as combinations of rotation, $\beta$-quadrupole and octupole vibrations, and $\gamma$-quadrupole vibrations. Instantaneous nuclear shapes that correspond to such excitations can be presented [12,13] in a body fixed system as

$$R(\theta', \varphi') = R_0 \left\{ 1 + \sum_{\lambda\mu} \beta_{\lambda\mu} Y_{\lambda\mu}(\theta', \varphi') \right\}. \tag{1}$$

Multipoles of deformed nuclear optical potentials are usually considered to arise from deformed instantaneous nuclear shapes of Eq. (1). We can expand such a potential with a deformed radius in a Taylor series considering the term $\sum_{\lambda\mu} \beta_{\lambda\mu} Y_{\lambda\mu}(\theta', \varphi')$ to be small,

$$V(r, R(\theta', \varphi')) = V(r, R_0) + \sum_{t=1}^{\max} \left. \frac{\partial^t V(r, R)}{\partial R^t} \right|_{R(\theta', \varphi') = R_0} \times \frac{R_0^t}{t!} \left( \sum_{\lambda\mu} \beta_{\lambda\mu} Y_{\lambda\mu}(\theta', \varphi') \right)^t, \tag{2}$$

in which the body fixed coordinates can be easily converted to the laboratory ones, that is,

$$Y_{\lambda\nu}(\theta', \varphi') = \sum_\nu D^{\lambda *}_{\mu\nu} Y_{\lambda\mu}(\theta, \varphi), \tag{3}$$

with the optical nuclear potential taken to be the standard form

$$V(r) = -V_R f_R(r) + i4W_D a_D \frac{d}{dr} f_D(r) - W_V f_V(r) + \left( \frac{\hbar}{\mu_\pi c} \right)^2 (V_{so} + i W_{so}) \frac{1}{r} \frac{d}{dr} f_{so}(r) \boldsymbol{\sigma} \cdot \mathbf{L} + V_{Coul}(r), \tag{4}$$

with the form factors of a Woods-Saxon type.

For the Coulomb potential $V_{Coul}(r)$, an expansion with evident dependences of deformations becomes possible as we follow the suggestion of Satchler *et al.* [14], using a multipole

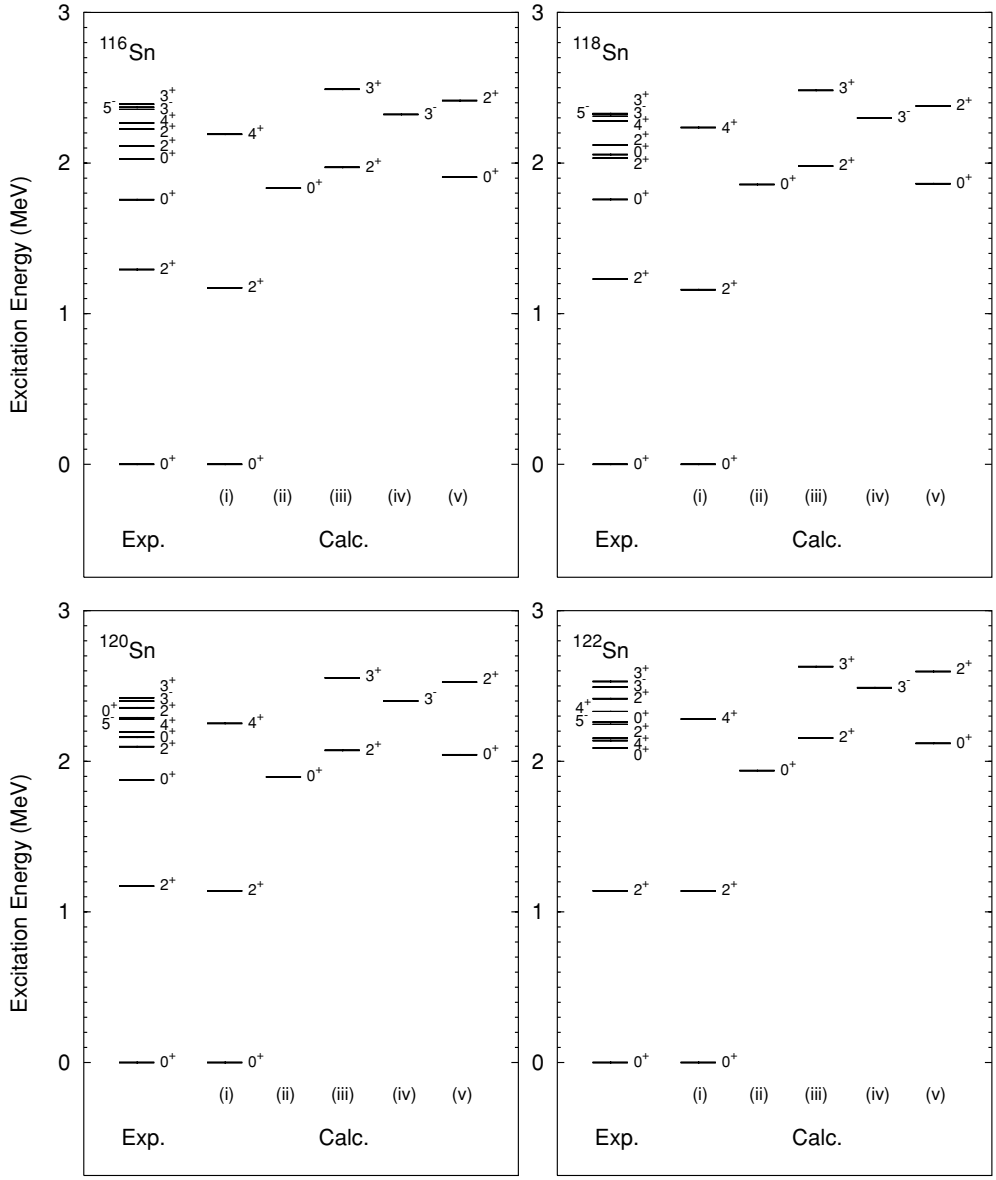


FIG. 1. Comparison of the theoretical and experimental nuclear levels for $^{116,118,120,122}$Sn nuclei. The experimental levels denoted with thin lines are not included in the present calculations. The Roman numbers denote the bands with the following quantum numbers: (i) $K \simeq 0, n_\gamma = n_{\beta_2} = n_{\beta_3} = 0$; (ii) $K \simeq 0, n_\gamma = n_{\beta_3} = 0, n_{\beta_2} = 1$; (iii) $K \simeq 2,\ n_\gamma = n_{\beta_2} = n_{\beta_3} = 0$; (iv) $K \simeq 0, n_\gamma = n_{\beta_2} = n_{\beta_3} = 0$; (v) $K \simeq 0, n_\gamma = 1, n_{\beta_2} = n_{\beta_3} = 0$.

expansion of the Coulomb potential $V_{\rm Coul}$ for the charged ellipsoid with a uniform charge density within the Coulomb radius $R_{\rm Coul}$. Up to the second order of $\sum \beta_{\lambda\mu} Y_{\lambda\mu}$, it becomes

$$
\begin{aligned}
V_{\rm Coul} = {} & \frac{ZZ'e^2}{2R_c}\left[3 - \frac{r^2}{R_c^2}\right]\theta(R_{\rm Coul} - r) + \frac{ZZ'e^2}{r}\theta(r - R_{\rm Coul}) \\
& + \sum_{\lambda\mu} \frac{3ZZ'e^2}{2\lambda + 1}\Big[r^\lambda R_{\rm Coul}^{-(\lambda+1)}\theta(R_{\rm Coul} - r) \\
& + R_{\rm Coul}^\lambda r^{-(\lambda+1)}\theta(r - R_{\rm Coul})\Big](\beta_{\lambda\mu} Y_{\lambda\mu}) \\
& + \sum_{\lambda\mu} \frac{3ZZ'e^2}{2\lambda + 1}\Big[(1 - \lambda)r^\lambda R_{\rm Coul}^{-(\lambda+1)}\theta(R_{\rm Coul} - r) \\
& + (\lambda + 2)R_{\rm Coul}^\lambda r^{-(\lambda+1)}\theta(r - R_{\rm Coul})\Big] \\
& \times \sum_{\lambda'\lambda''} \frac{\hat\lambda'\hat\lambda''}{(4\pi)^{1/2}\hat\lambda}(\lambda'\lambda''00 \mid \lambda 0) \sum_\mu (\beta_{\lambda'} \otimes \beta_{\lambda''})_{\lambda\mu}\, Y_{\lambda\mu},
\end{aligned}
\tag{5}
$$

where $\hat\lambda = (2\lambda + 1)^{1/2}$, while the symbol $\otimes$ means vector addition, i.e.,

$$
(\beta_{\lambda'} \otimes \beta_{\lambda''})_{\lambda\mu} = \sum_{\mu'\mu''} (\lambda'\lambda''\mu'\mu'' \mid \lambda\mu)\beta_{\lambda'\mu'}\beta_{\lambda''\mu''}, \tag{6}
$$

and $\theta(r) = 1$ if $r > 0$ and $\theta(r) = 0$ if $r < 0$.

The Coulomb potential used in the present work introduces some modifications to Eq. (5). The spherical term in Eq. (5) is calculated taking into account the diffuseness of the charge

distribution. Because our model involves quadrupole, octupole, and hexadecapole instantaneous nuclear deformations, the expansion of the Coulomb potential can in principle result in additional coupling strength between collective states with angular momentum transfer of 0 to 8. However, in expanding the Coulomb potential, we truncate the dynamic square terms which lead to zero angular momentum transfer. This is equivalent to introducing a dynamic negative deformation $\beta_{00}$ in the radial expansion given in Eq. (1),

$$\beta_{00} = -\sum_{\lambda}(-1)^{\lambda}\frac{\hat{\lambda}}{(4\pi)^{1/2}}(\beta_{\lambda}\otimes\beta_{\lambda})_{00}\,, \tag{7}$$

which is required as a condition to conserve the nuclear volume, i.e., the nuclear charge [15]. This correction is necessary to have the right asymptotic behavior for the spherical term of the Coulomb potential, which must be equal to $ZZ'e^2/r$. The additional coupling due to the Coulomb potential is obtained in the same manner as for the nuclear one [6] with deformed radii as described above.

Since we intend to analyze the interaction data in a wide energy region (at least up to 200 MeV incident energies) for both neutrons and protons simultaneously, we use a global form of the optical potential which incorporates the energy dependence of the potential derived from the dispersion relation of Delaroche *et al.* [16] and the high-energy saturation behavior consistent with the Dirac phenomenology. The imaginary components of this potential form vanish at Fermi energy, a property stemming from nuclear matter theory. Such an energy dependence allows data analysis without unphysical discontinuities in the whole energy range of interest for both neutrons and protons:

$$V_R = \left(V_R^0 + V_R^{\rm disp}e^{-(\lambda_{1R}E^*+\lambda_{2R}E^{*2}+\lambda_{3R}E^{*3})}\right) \times\left(1+\frac{1}{V_R^0+V_R^{\rm disp}}(-1)^{Z'+1}C_{\rm viso}\frac{A-2Z}{A}\right) \tag{8}$$

$$+C_{\rm Coul}\frac{ZZ'}{A^{1/3}}\varphi_{\rm Coul}(E^*), \tag{9}$$

$$W_D = \left[W_D^{\rm disp}+(-1)^{Z'+1}C_{\rm wiso}\frac{A-2Z}{A}\right]e^{-\lambda_D E^*} \times\frac{E^{*2}}{E^{*2}+B_D^2}, \tag{10}$$

$$W_V = W_V^{\rm disp}\frac{E^{*2}}{E^{*2}+B_V^2}, \tag{11}$$

$$V_{\rm so} = V_{\rm so}^0 e^{-\lambda_{\rm so}E^*}, \tag{12}$$

$$W_{\rm so} = W_{\rm so}^{\rm disp}\frac{E^{*2}}{E^{*2}+B_{\rm so}^2}. \tag{13}$$

Here $B_i$ ($i = D, V$, and so) denotes a width of the imaginary dispersive potentials and $E^* = (E_p - E_{\rm fm})$, with $E_p$ the energy of the projectile and $E_{\rm fm}$ the Fermi energy, determined to be $E_{\rm fm}(Z,A) = -\frac{1}{2}[S_n(Z,A)+S_n(Z,A+1)]$ for neutrons and $E_{\rm fm}(Z,A) = -\frac{1}{2}[S_p(Z,A)+S_p(Z+1,A+1)]$ for protons. Here, $S_i(Z,A)$ denotes a separation energy of nucleon $i$ from a nucleus, while $Z'$, $Z$ and $A$ are charges of incident particle and nucleus and nuclear mass number, respectively. Since we intend to analyze neutron and proton scattering data simultaneously, we keep unique optical potentials for nucleons with a form suggested by Ref. [16] plus a term $C_{\rm Coul}ZZ'/A^{1/3}\varphi_{\rm Coul}(E^*)$ describing the Coulomb correction to the real optical potential and isospin terms added to the real $(-1)^{Z'+1}C_{\rm viso}(A-2Z)/A\varphi_{\rm viso}(E^*)$ and imaginary $(-1)^{Z'+1}C_{\rm wiso}(A-2Z)/A\cdot\varphi_{\rm wiso}(E^*)$ surface potentials. We assume that the dependences on the initial energy of the real potential isospin term $\varphi_{\rm viso}(E^*)$ and imaginary isospin term $\varphi_{\rm wiso}(E^*)$ follow the rate of real and imaginary surface potential energy dependence [see Eqs. (8) and (10)], while $\varphi_{\rm Coul}(E^*)$ is considered to be the negative of the derivative of Eq. (8), so that

$$\varphi_{\rm Coul}(E_p) = (\lambda_{1R}+2\lambda_{2R}E^*+3\lambda_{3R}E^{*2}) \times V_R^{\rm disp}e^{-(\lambda_{1R}E^*+\lambda_{2R}E^{*2}+\lambda_{3R}E^{*3})} \times\left(1+\frac{1}{V_R^0+V_R^{\rm disp}}(-1)^{Z'+1}C_{\rm viso}\frac{A-2Z}{A}\right). \tag{14}$$

All potential parameters are taken to be equal for neutrons and protons. We consider that the Lane model [17] is valid, and therefore the neutron-proton optical potential difference of the suggested potential stems from the isospin terms, from the Coulomb correction added to the real central potential, and from the neutron-proton Fermi energies.

Since energy losses due to the collective excitation of levels are expected to be non-negligible compared to the nucleon incident energies, the dependence of the local optical potential for different channels is taken into account, i.e.,

$$V_{if} = V\left(E_p - \frac{E_i+E_f}{2}\right),$$

where $E_i$ and $E_f$ are the corresponding energy levels of initial and final channels, respectively. And our nonrelativistic Schrödinger formalism takes into account relativistic generalization suggested by Elton [18]. The nucleon wave number $k$ is taken in the relativistic form

$$(\hbar k)^2 = [E^2 - (M_pc^2)^2]/c^2,$$

where $E$ denotes the total energy of the projectile, $M_p$ the projectile rest mass, and $c$ the speed of light. To allow nonrelativistic motion of the target with rest mass $M_T$, incident particle mass $M_p$ is changed by relativistic projectile energy $E$ in the reduced mass formula, so that the quantity $k$ and optical potential values are multiplied by a coefficient:

$$\frac{1}{1+E/(M_Tc^2)}.$$

Following Elton's [18] suggestions, we multiply the optical potential values (except the spin-orbit component) by a factor $K(E)$, as a relativistic generalization of the optical potential behavior; Elton [18] suggests $K(E) = E/(M_pc^2)$. However, this factor increases without limit as the projectile energy $E$ increases. We alternatively use the factor suggested by Madland [19], $K(E) = 2E/(E+M_pc^2)$, which saturates at the value of 2 as incident energy grows, as it is more physical and allows easier fitting of experimental data. Of course, optical potentials can, in any case, be fit to the experimental data without such a multiplier, so that a relativistic correction can be included in the fit. However, we agree with Elton [18]

that "it is advantageous to separate out known relativistic factor in the central potential," as this may allow successful extrapolation of optical potential from a low incident projectile energy region to higher and *vice versa*. One can see that for low energies, all these relativistic generalization factors have the nonrelativistic kinematic limit.

### B. Optical model calculations

Nuclear wave functions from the soft-rotator model with the parameters for the nuclear Hamiltonian given in Table I adjusted to describe the energies of low-lying collective levels, are used for our CC calculations. Specifically, we couple the collective levels $0^+$(g.s.), $2_1^+$, $0_2^+$, $2_2^+$, $3_1^-$, and $4_1^+$, in our CC optical model calculations. Positive parity levels with $J^\pi = 0_3^+, 2_3^+$ of $K \simeq 0, n_\beta = 0, n_\gamma = 1$, and $J^\pi = 3_1^+$ of $K \simeq 2$, $n_\beta = n_\gamma = 0$ are not used in the CC optical calculations, as they change the results much less than experimental errors.

In our calculations, pairs of the levels having the same parity and levels themselves are coupled by all possible even multipoles with angular momentum transfer up to $8\hbar$, and pairs of levels with different parity are coupled by odd multipoles with angular momentum transfer up to $7\hbar$. The Coulomb interaction enhances the coupling in all the pairs of levels except between $0^+$ and $0_2^+$ states (as square terms that lead to Coulomb potential zero multipoles are truncated), so these levels are coupled by the nuclear potential only. We emphasize that in our model, levels from various bands are coupled not only with the g.s. band but also with each other without any additional assumptions. Such a feature is absent in most of the previous analyses.

Optical potential parameters were determined by minimizing the quantity $\chi^2$ defined by

$$\chi^2 = \frac{1}{N+M}\left[\sum_{i=1}^{N}\frac{1}{K_i}\sum_{j=1}^{K_i}\left(\frac{d\sigma_{ij}^{\rm calc}/d\Omega - d\sigma_{ij}^{\rm exp}/d\Omega}{\Delta\sigma_{ij}^{\rm exp}/d\Omega}\right)^2 + \sum_{i=1}^{M}\left(\frac{\sigma_{{\rm tot},i}^{\rm calc} - \sigma_{{\rm tot},i}^{\rm eval}}{\Delta\sigma_{{\rm tot},i}^{\rm eval}}\right)^2\right], \quad (15)$$

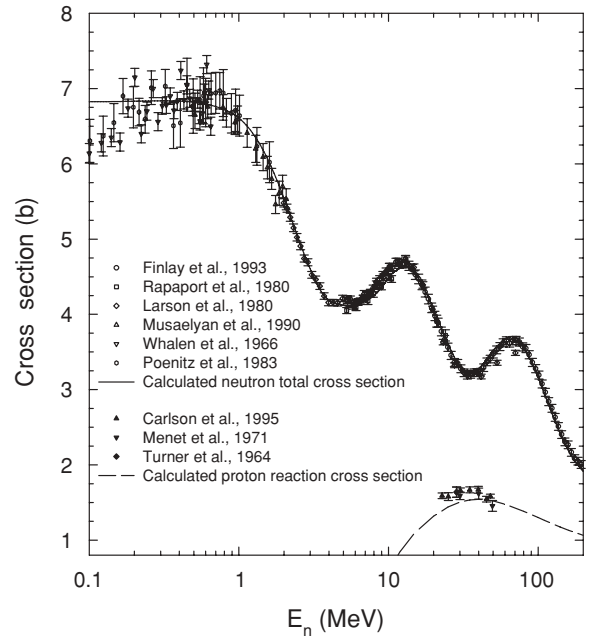


FIG. 2. Comparison of the theoretical and experimental total neutron (open points and solid line) and proton (solid points and dashed line) cross sections for $^{120}$Sn up to 200 MeV neutron incident energy.

where $N$ is the number of experimental scattering data sets, $K_i$ number of angular points in each data set, $M$ number of energies, for which evaluated total neutron cross section is available. The final overall $\chi^2$ is 3.8, 10.3, 5.7, and 4.7 for $^{116}$Sn, $^{118}$Sn, $^{120}$Sn, and $^{122}$S, respectively. This indicates that the experimental data are described within approximately 1.9, 3.2, 2.4, and 2.2 standard deviations, respectively. In searching for the optical potential parameters, all the nuclear Hamiltonian parameters are fixed as in Table I. The resultant optical potential parameters, allowing the best fit to the experimental data, are presented in Table II. The parameters are essentially the same for all Sn isotopes except

TABLE II. Optical potential parameters for the Sn isotopes allowing the best fit with the experimental data. Potential strengths are in MeV; radii and diffusenesses in fm. Note that optical potential strengths, except for the spin-orbit and Coulomb terms, must be multiplied by a factor $K(E) = 2E/(E + M_p c^2)$ due to the relativistic generalization as discussed in the text.

| | | |
|---|---|---|
| $V_R^0 = -35.59–0.025A$ | $V_R^{\rm disp} = 93.96$ | |
| $\lambda_{1R} = 0.003904$ | $\lambda_{2R} = -0.00000054$ | $\lambda_{3R} = 0.000000031$ |
| $W_D^{\rm disp} = 13.89$ | $B_D = 11.15$ | $\lambda_D = 0.0665$ |
| $W_V^{\rm disp} = 15.12$ | $B_V = 80.64 + 0.085A$ | |
| $V_{\rm so}^0 = 6.2$ | $\lambda_{\rm so} = 0.005$ | |
| $W_{\rm so}^{\rm disp} = -3.1$ | $B_{\rm so} = 160.00$ | |
| $r_R = 1.2058$ | $a_R = 0.654$ | |
| $r_D = 1.2393$ | $a_D = 0.580$ | |
| $r_V = r_R = 1.2058$ | $a_V = a_R = 0.654$ | |
| $r_{\rm Coul} = 1.2518$ | $a_{\rm Coul} = 0.340$ | |
| $C_{\rm Coul} = 1.27$ | $C_{\rm viso} = 16.0$ | $C_{\rm wiso} = 23.0$ |
| $r_{\rm so} = 1.0837$ | $a_{\rm so} = 0.59$ | |

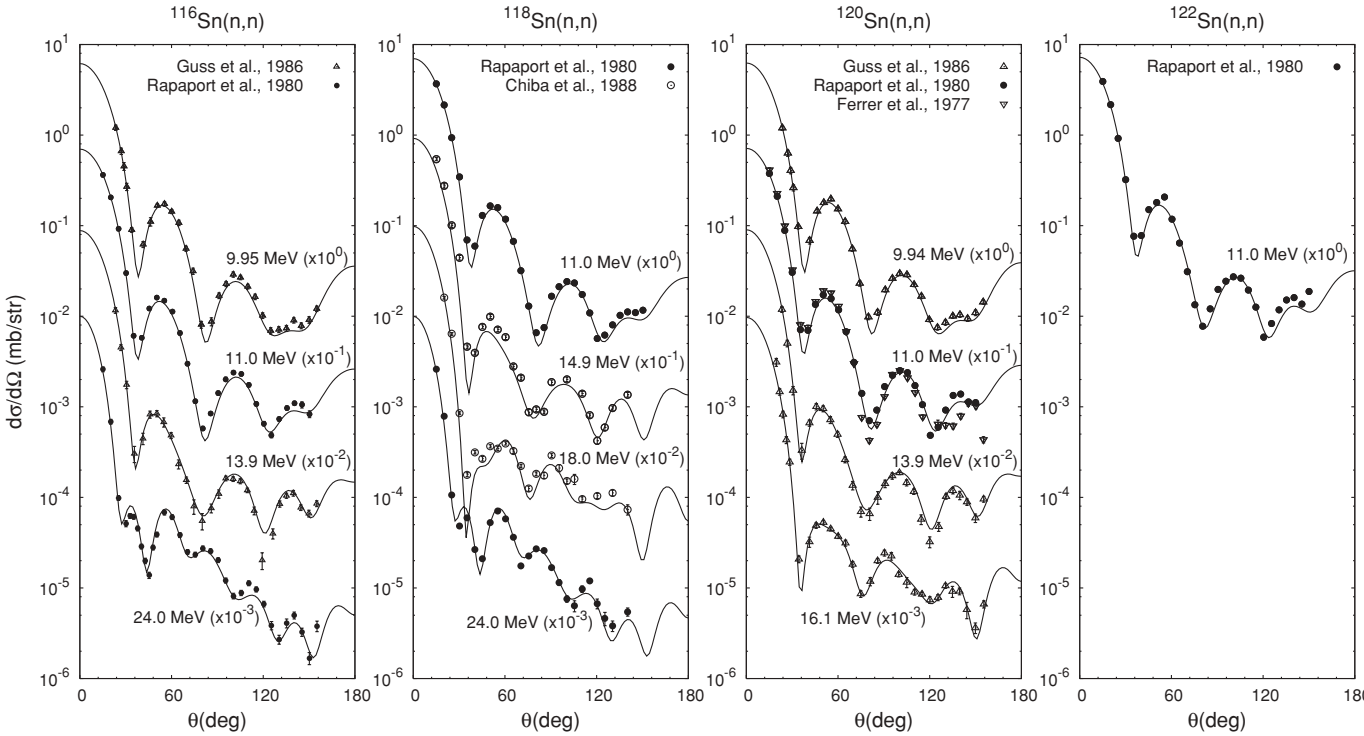


FIG. 3. Comparison of the theoretical and experimental angular distributions for neutrons elastically scattered by $^{116,118,120,122}$Sn. The solid lines denote the calculated results.

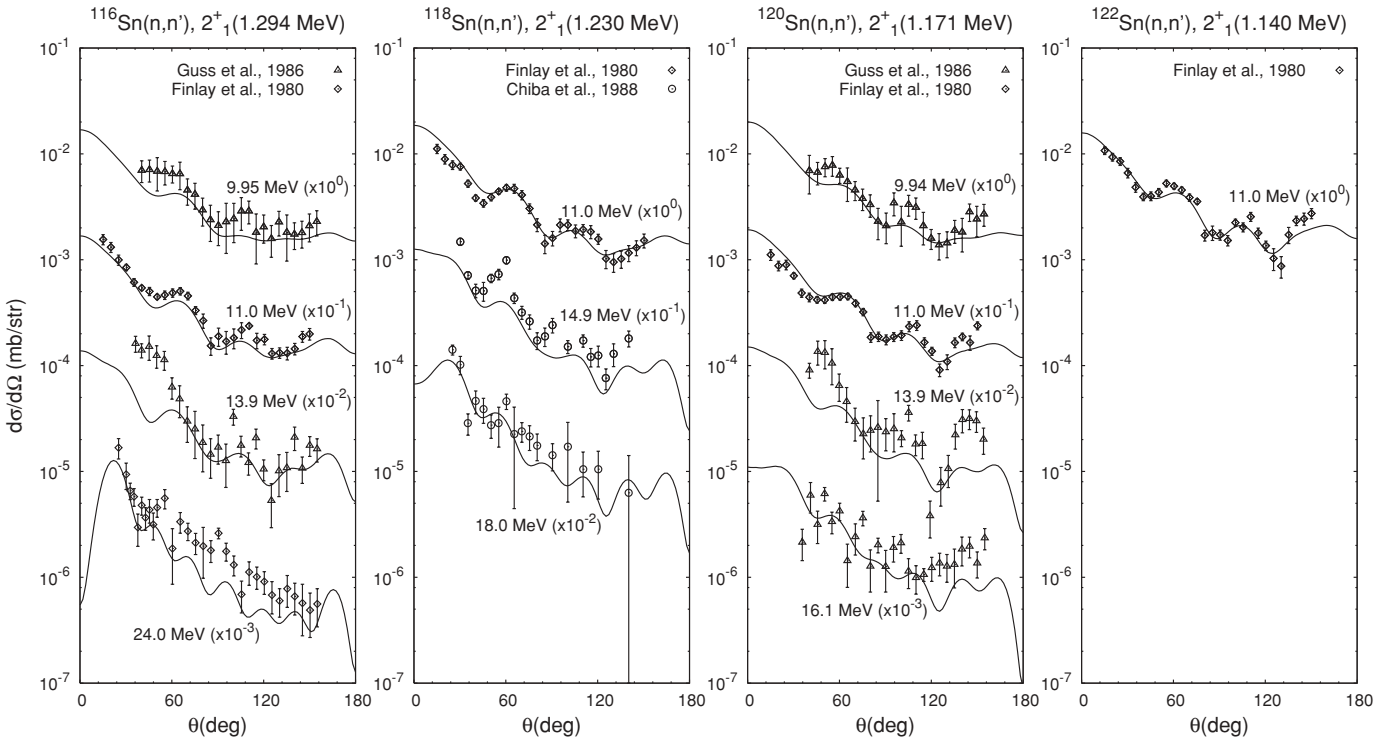


FIG. 4. Comparison of the theoretical and experimental angular distributions for neutrons scattered with $2_1^+$ level excitations of $^{116,118,120,122}$Sn.

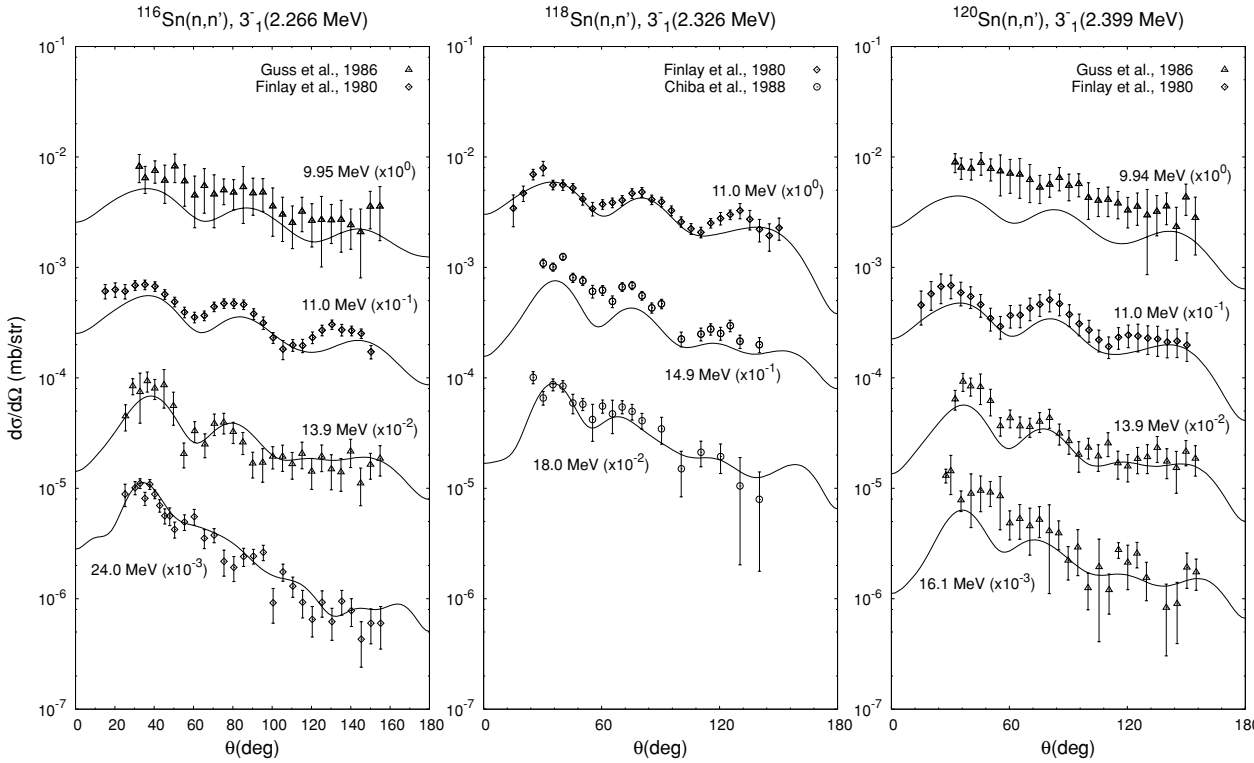


FIG. 5. Comparison of the theoretical and experimental angular distributions for neutrons scattered with $3^-_1$ level excitations of $^{116,118,120}$Sn.

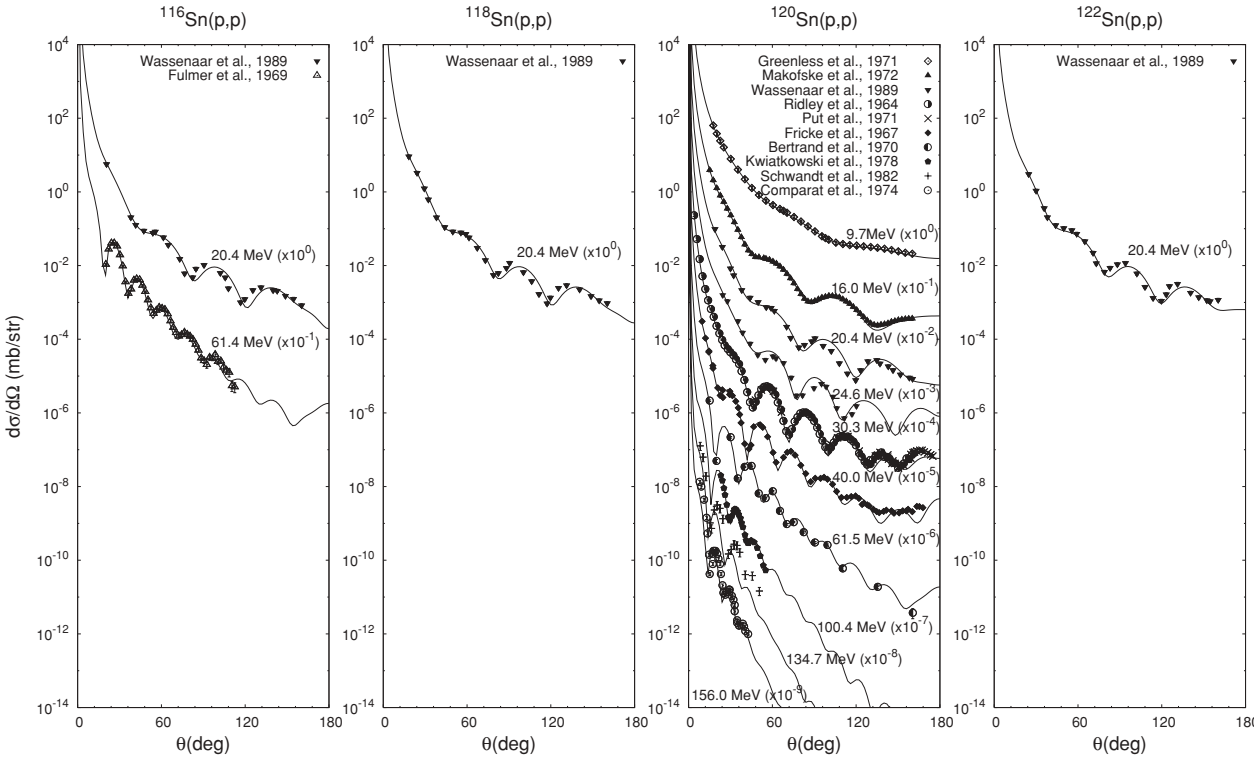


FIG. 6. Comparison of the theoretical and experimental angular distributions for protons elastically scattered by $^{116,118,120,122}$Sn.

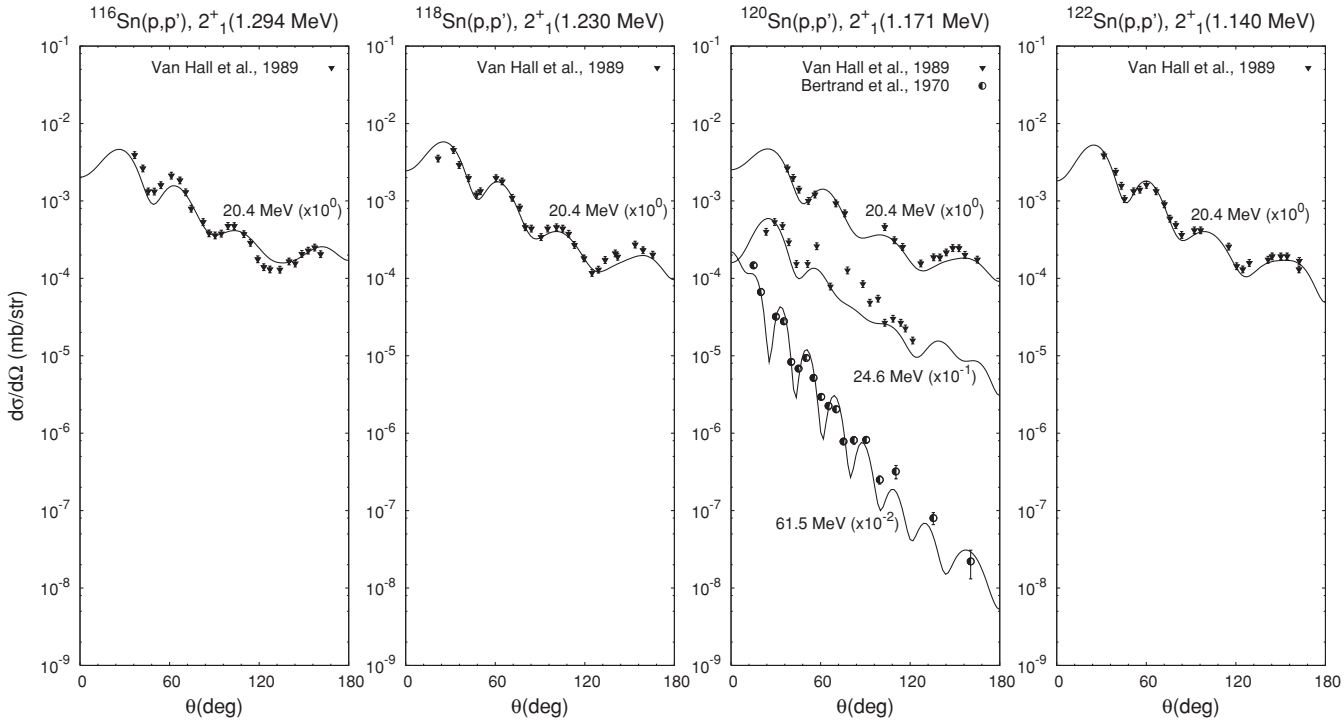


FIG. 7. Comparison of the theoretical and experimental angular distributions for protons scattered with $2_1^+$ level excitations of $^{116,118,120,122}$Sn.

for a small dependence of $V_R^0$ and $B_V$ on the mass number. We do not include scattered angular distribution data for low nucleon interaction energies (lower than 7 MeV) in the adjustment, because we cannot guarantee that the compound interaction contribution to angular distributions is less than the experimental errors and can be neglected. At the higher energies considered, we therefore assume that the interactions of nucleons with Sn isotopes proceed completely via a direct mechanism, which can be described by the optical model.

Figure 2 shows the calculated total neutron cross sections for $^{120}$Sn compared with the experimental data from 0.1 to 200 MeV incident energy for natural Sn [20]. Such comparison is reasonable because $^{120}$Sn has the highest abundance in natural Sn (about 34%) and total cross sections are to be smoothly proportional to $A^{1/3}$. One can see that theoretical results are in good agreement with the experimental data over the energy range. Proton reaction cross sections are also shown in Fig. 2. We see that available experimental proton reaction cross sections as well as the total neutron cross sections are reasonably well described by using our potential.

Figure 3 shows the angular distributions for the neutron elastic scattering cross sections for four tin isotopes, $^{116,118,120,122}$Sn. We can state that the soft-rotator approach allows us to describe the angular distributions for the elastically scattered neutrons.

Figure 4 shows the angular distributions of the cross sections for the neutron inelastic scatterings leading to the $2_1^+$ excitation energies of $^{116,118,120,122}$Sn. For the most incident energies, the calculated results show good agreement with experimental data.

Figure 5 shows the angular distributions of the cross sections for the neutron inelastic scatterings leading to the $3_1^-$ excitation energies of $^{116,118,120}$Sn. For $^{120}$Sn, we underestimate angular distributions for neutron incident energy 9.993 MeV, probably because the compound process contribution to this excitation was not accounted for. This difference disappears at higher incident energies where such compound contributions vanish.

Figure 6 compares our calculations and the available experimental data for protons elastically scattered by $^{116,118,120,122}$Sn. One can see that the elastic scattering data are well described almost within errors for proton incident energies from 9.7 to 156 MeV.

Figure 7 shows the angular distributions of the cross sections for the inelastic scatterings leading to the $2_1^+$ excitation energies of $^{116,118,120,122}$Sn up to 61.5 MeV. The calculated results show good agreement with experimental data over the considered energy regions.

Figure 8 shows the angular distributions of the cross sections for the inelastic scatterings leading to the $3_1^-$ excitation energies of $^{116,118,120,122}$Sn. The calculated results are also in good agreement with experimental data over the wide incident energy regions from 20 to 61.5 MeV.

We mentioned above that we cannot describe the energy sequence of $5_1^-$ levels of Sn isotopes because they are observed at energies lower than those of $3_1^-$ levels. Nevertheless, we tried to describe available experimental angular scattering data with excitation of $5_1^-$ level of $^{122}$Sn, adding it to the coupling scheme. Figure 9 compares such calculated results and experiment data. Though predicted values are by a factor of 2 lower than the experimental data for scattering angles lower than 60°, they can describe the experimental data for the higher angles. We can conclude that the overall shape of the theoretical angular distributions for the proton inelastic

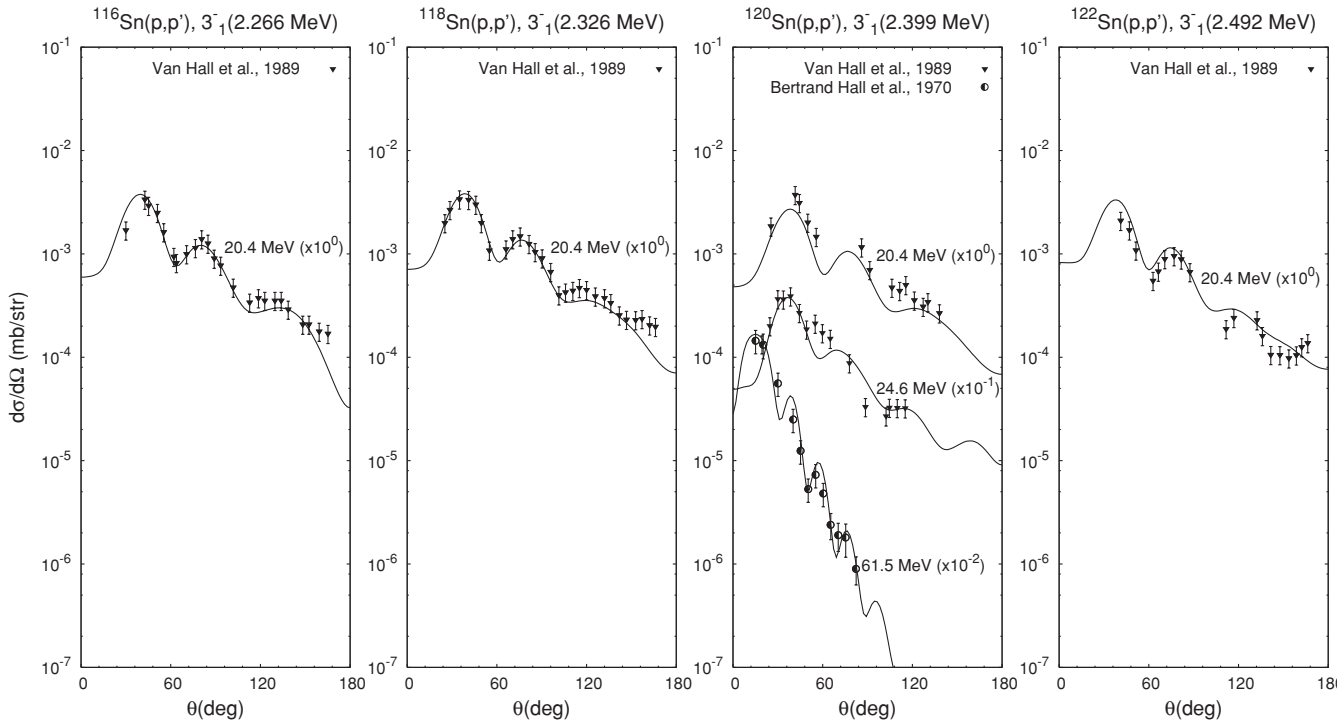


FIG. 8. Comparison of the theoretical and experimental angular distributions for protons scattered with $3_1^-$ level excitations of $^{116,118,120,122}$Sn.

scatterings leading to $5^-$ excitation energy is almost the same as the one of the corresponding experiment data.

## IV. ANALYSES OF Sn NUCLEI $\beta_2$ AND DEFORMATION DIFFERENCES FOR PROTON AND NEUTRON PROBES

It was predicted that the measured deformation for proton (neutron) closed-shell nuclei would increase when the nucleus is probed with protons (neutrons) compared to the measurements with neutrons (protons) [2]. Sn isotopes are proton closed-shell nuclei. To check this theoretical prediction, we determine the best fit values for $\beta_2$ and $\beta_3$ deformations with incident protons and neutrons. Since we perform a consistent coupled-channels optical model calculation using the strongly coupled levels, we can simultaneously distinguish the differences in both $\beta_2$ and $\beta_3$ deformations, free from any errors associated with the missing coupling strength. Deformations allowing the best fit for incident protons and neutrons are presented in Table III; these are equilibrium values and to obtain the "effective" deformation values, they must be multiplied by enhancement factors [6,8], which are 4.25, 4.41; 3.89, 3.86; 3.39, 3.52; and 3.06, 3.15 for $\beta_2$, $\beta_3$ deformations for $^{116}$Sn, $^{118}$Sn, $^{120}$Sn, and $^{122}$Sn, respectively. The relative ratios of effective deformation values for neutrons and protons are, however, the same as for the equilibrium ones.

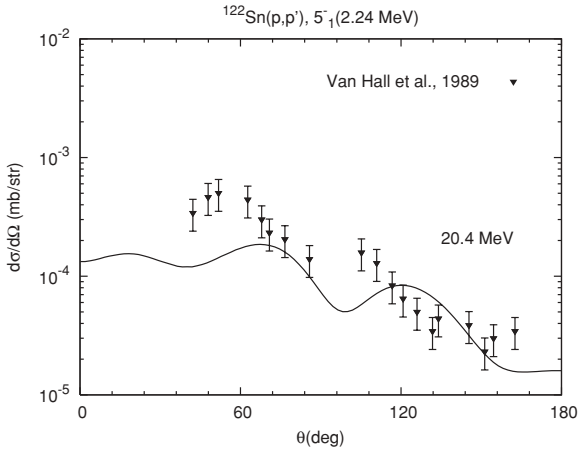


FIG. 9. Comparison of the theoretical and experimental angular distributions for protons scattered with $5_1^-$ (2.240 MeV) level excitation of $^{122}$Sn.

We do find that the $\beta_2$ deformations for all Sn isotopes are higher for incident protons than for neutrons as the incident probe: the average $\beta_2$ difference for $^{116}$Sn, $^{118}$Sn, and $^{120}$Sn is about 15%, while $\beta_3$ for these Sn isotopes is also higher by about 5%. $\beta_2$ deformations determined in the present work are much more accurate than those calculated with a DWBA approach and more accurate than those calculated via simpler CC calculations. For example, a CC calculation of $^{118}$Sn [21]

TABLE III. Deformation parameters of Sn isotopes allowing the best fit with the experimental data.

| Nuclide | $\beta_{20}$ | | $\beta_{30} = \beta_{20}\epsilon_0$ | | $\beta_{40}$ |
|---|---|---|---|---|---|
| | Neutrons | Protons | Neutrons | Protons | |
| $^{116}$Sn | 0.0246 | 0.0267 | 0.0504 | 0.0526 | −0.080 |
| $^{118}$Sn | 0.0291 | 0.0345 | 0.0471 | 0.0489 | −0.060 |
| $^{120}$Sn | 0.0336 | 0.0364 | 0.0433 | 0.0447 | −0.094 |
| $^{122}$Sn | 0.0347 | 0.0452 | 0.0350 | 0.0588 | −0.012 |

used a simple coupling scheme that ignored the contribution of $\beta_3$ deformations to the coupling of $0^+$(g.s.) with $2_1^+$ level. This coupling is needed for a consistent approach, as it gives rise to a second-order expansion of deformed radii $\beta_{2\mu} \sim (\beta_3 \otimes \beta_3)_{2\mu}$ and two step excitation through the $3^-$ level. Determinations of $\beta_3$ deformations in our work are much more accurate for the same reasons. While a 5% increase of $\beta_3$ for protons is close to the accuracy of our calculation, we still conclude that $\beta_3$ has the same tendency to increase as $\beta_2$, but the impact of the closed shell on it is very small.

Our calculated $^{122}$Sn neutron-proton $\beta_2$ and $\beta_3$ deformation differences have the same tendency, but with a much larger effect: 30% and 60%, respectively. For $^{122}$Sn, our results are not so accurate, as they are based on experimental neutron and proton measurements with a single incident energy. Furthermore, for the neutron experimental scattering data, the $3^-$ level excitation is unavailable, so the $\beta_3$ deformation for incident neutrons is determined by the impact on the elastic and $2_1^+$ level excitation. As mentioned above, our consistent CC approach allows this, but this approach leads to significantly larger uncertainties in $\beta_3$ values for $^{122}$Sn.

For a $^{118}$Sn nucleus, we can compare the effective $\beta_2$ and $\beta_3$ deformations determined in the present work with those of earlier works [21–23]. Our calculated effective $\beta_2$ for neutrons is 0.113, while it was determined to be 0.115 in Ref. [21]; for protons, our calculated effective $\beta_2$ is 0.133, whereas it was 0.134 in Refs. [22,23]. And our effective $\beta_3$ for neutrons is 0.183, while it was 0.172 in Ref. [21]; for protons, our calculated effective $\beta_3$ is 0.189, while it was 0.174 in Ref. [23]. One can see that our calculated $\beta_2$ values agree very well with the previous works, while the present work $\beta_3$ values are 6% greater than the old ones. This can be understood because their $3^-$ level analyses [23] were based on DWBA calculations. In the absence of $2^+$ level couplings, predictions of the $3^-$ level excitation result in a lower value of $\beta_3$.

## V. CONCLUSIONS

The CC calculations based on the soft-rotator nuclear Hamiltonian wave functions are applied to simultaneously analyze all data available for Sn even-even isotopes including nuclear level structure, total neutron cross sections, and nucleon elastic and inelastic scattering cross sections. The non-axial quadrupole, octupole, and hexadecapole deformations, and quadrupole and octupole vibrations are taken into account in this soft-rotator model. Furthermore, our soft-rotator model is self-consistent, since the parameters of the nuclear Hamiltonian are determined by adjusting the energies of collective levels to the nuclear structure data prior to the optical model calculation. The nuclear level energies for the four Sn isotopes are predicted using the soft-rotator model, analyzed, and compared with the experimental ones. For each Sn isotope, we can describe nine collective levels out of approximately 10–12 levels observed below 2.4 MeV in excitation energy. For all these isotopes, we are not able to describe the energy sequence of $5_1^-$ levels, which are observed at energies lower than $3_1^-$ ones. Theoretically predicted energies of Sn levels other than $5_1^-$ are in good agreement with the experimental ones. It is also found that rotational structures are not very prominent in Sn isotopes. Nevertheless, for each isotope, we can describe at least the first five low-lying collective levels, with average energy prediction accuracy better than 5%, as well as numerous higher-lying levels which are necessary for coupled-channel cross section calculations. In addition, all the nucleon interaction data available, including total neutron cross sections and nucleon elastic and inelastic scattering data, are well described within such a unified approach up to 200 MeV incident energies with unique optical potential parameters. Isotopes are described by individual nuclear Hamiltonian parameters, Fermi energies, deformations, and $Z, N$ potential dependencies. Analyses show that $\beta_2$ deformation for incident protons is 15% higher than that for incident neutrons, which is consistent with theoretical predictions for proton closed-shell nuclei such as Sn. $\beta_3$ deformation shows the same tendency. Our approach seems useful for analyses of nucleon interactions with nuclei in a wide atomic mass region by using global optical model potentials.

## ACKNOWLEDGMENTS

The authors are grateful to Dr. Yutaka Utsuno for discussions on the nuclear structure aspect. This work was supported by the Korea Research Foundation Grant funded by the Korean Government (MOEHRD, Basic Research Promotion Fund) (KRF-2005-070-C00034), WCU Program (R31-2008-000-10029-0), and BAERI Program (M20608520001-08B0852-00110) funded by the Ministry of Education, Science and Technology through the Korea Science and Engineering Foundation.

[1] T. Tamura, Rev. Mod. Phys. **37**, 679 (1965).
[2] V. A. Madsen, V. R. Brown, and J. D. Anderson, Phys. Rev. C **12**, 1205 (1975).
[3] Y. V. Porodzinskij and E. Sh. Soukhovitskii, Sov. J. Nucl. Phys. **54**, 570 (1991).
[4] Y. V. Porodzinskij and E. Sh. Soukhovitskii, Phys. At. Nucl. **59**, 228 (1996).
[5] E. Sh. Soukhovitskii, O. Iwamoto, S. Chiba, and T. Fukahori, J. Nucl. Sci. Technol. **37**, 120 (2000).
[6] S. Chiba, O. Iwamoto, Y. Yamanouti, M. Sugimoto, M. Mizumoto, K. Hasegawa, E. Sh. Soukhovitskii, Y. V. Porodzinskij, and Y. Watanabe, Nucl. Phys. **A624**, 305 (1997).
[7] S. Chiba, O. Iwamoto, E. Sh. Soukhovitskii, Yu. Watanabe, and T. Fukahori, J. Nucl. Sci. Technol. **37**, 498 (2000).
[8] E. Sh. Soukhovitskii, Y.-O. Lee, J. Chang, S. Chiba, and O. Iwamoto, Phys. Rev. C **62**, 044605 (2000).
[9] J. Y. Lee, E. Sh. Soukhovitskii, Y.-O. Lee, J. Chang, S. Chiba, and O. Iwamoto, J. Korean Phys. Soc. **38**, 88 (2001).
[10] E. Sh. Soukhovitskii, S. Chiba, J. Y. Lee, B. T. Kim, and S. W. Hong, J. Nucl. Sci. Technol. **40**, 69 (2003).
[11] E. Sh. Soukhovitskii, S. Chiba, J. Y. Lee, Y.-O. Lee, J. Chang, T. Maruyama, and O. Iwamoto, J. Nucl. Sci. Technol. **39**, 816 (2002).

[12] A. Bohr and B. R. Mottelson, *Nuclear Structure* (Benjamin, New York, 1975), Vol. II, p. 195.
[13] A. S. Davydov, *Vozbuzhdennye sostoyaniya atomnykh yader (Excited States of Atomic Nuclei)* (Atomizdat, Moscow, 1969).
[14] R. H. Bassel, R. M. Drisko, and G. R. Satchler, Oak Ridge National Laboratory Report, ORNL-3240, 1962 (unpublished).
[15] J. M. Eisenberg and W. Greiner, *Nuclear Models* (North-Holland, Amsterdam, 1970).
[16] J. P. Delaroche, Y. Wang, and J. Rapaport, Phys. Rev. C **39**, 391 (1989).
[17] A. M. Lane, Phys. Rev. Lett. **8**, 171 (1962); Nucl. Phys. **35**, 676 (1962).
[18] R. L. B. Elton, Nuovo Cimento **43B**, 277 (1966).
[19] D. G. Madland and A. J. Sierk, in *Proceedings of the International Conference on Nuclear Data for Science and Technology, Trieste, 1997,* edited by G. Reffo, A. Ventura, and C. Grandi (Italian Physical Society, Bologna, Italy, 1997), Vol. 1, p. 202.
[20] F. S. Dietrich *et al.*, in *Proceedings of the International Conference on Nuclear Data for Science and Technology, Trieste, 1997,* edited by G. Reffo, A. Ventura, and C. Grandi (Italian Physical Society, Bologna, Italy, 1997), Vol. 1, p. 402.
[21] S. Chiba *et al.*, J. Nucl. Sci. Technol. **25**, 511 (1988).
[22] W. Makovske, W. Savin, H. Ogata, and T. H. Kruse, Phys. Rev. **174**, 1429 (1966).
[23] O. Beer *et al.*, Nucl. Phys. **A147**, 326 (1970).